Available online at http://arjournal.org

APPLIED RESEARCH JOURNAL

RESEARCH ARTICLE

ISSN: 2423-4796

Applied Research Journal *Vol.1, Issue, 3, pp.127-136, May, 2015*

FIRST-PRINCIPLE INVESTIGATION OF DOPING EFFECTS ON ELECTRONIC, ELASTIC, THERMAL AND OPTICAL PROPERTIES OF $CoFe_2O_4$

M. A. Rahman, M. M. Hossain, M. S. Islam, *M. A. R. Sarker

Department of Physics, University of Rajshahi, Bangladesh.

ARTICLE INFO

Article History:

Received: 11, April, 2015
Final Accepted: 13, May, 2015
Published Online: 15, May, 2015

Key words:

Elastic properties, Electronic properties, GGA, Optical properties, Thermal properties.

ABSTRACT

The oxides with spinel structure are interesting materials responsible for useful device applications due to their promising chemical and physical properties achievable in accommodation of foreign citations. Partial substitution of iron with transition metals like Zn, Zr, Cd in CoFe2O4 might change their structural, electronic, optical and thermal properties that influence various applications. The first principle ab initio study of on the doping effect of such transition metal elements in cobalt ferrite has been performed in this work. The bulk modulus and ductility of CoFe2O4 are 233 GPa and 0.21 where as that of CoFe1.8Cd0.2O4 are reported to be 251 GPa and 0.14 respectively. The Debye temperature of CoFe2O4 increase with pressure but that of CoFe1.8Zn0.2O4 is reported to be almost constant with pressure. The pressure dependence Cv and Cp of CoFe1.8Zn0.2O4 also shows anomalous behavior.

1. INTRODUCTION

The spinel structure of oxides with cationic tetrahedral (A) and octahedral (B) sites of the general formula AB_2O_4 is responsible for a variety of physical and chemical properties. Such specialty in properties is achieved through accommodation of different cations, among the A and B sites, sometimes in more than one oxidation state. This kind of multi-valence is possible due to the partially filled nature of transition-metal 3d orbitals. A wide range of work on structural and magnetic characterization of spinel ferrite in the form of nano-size has been done by many workers [1]-[2]. Among the different spinel ferrites cobalt ferrite ($CoFe_2O_4$) with inverse spinel structure covered a wide range of applications including electronic devices, high density information storage devices, high rate of change of strain with magnetic field, good electrical insulation etc. [2]-[8]. Cobalt ferrites have recently attracted more and more attention due to the combination of properties usually associated with metals and ceramics. This type of ceramics possesses metal-like properties such as high Young's modulus, good thermal and electrical conductivity. This material are exceptionally damage tolerant, remarkably ductile and easily machinable by conventional cutting tools which make them technologically interesting materials. The unique combination of metallic and ceramic properties makes them suitable for possible applications in a variety of high temperature applications or in other extreme environments. A lot of theoretical studies [9]-[13] have focused on ideal inverse and normal spinels of $CoFe_2O_4$ by the local spin density approximation (LSDA) [9]-[10]. In this work we mainly apply the generalized gradient approximation (GGA) to study the different properties of $CoFe_2O_4$. Some transition metals were doped in iron site of the cobalt ferrite [$CoFe_{2-x}M_xO_4$, M=Zn, Zr, Cd] to enhance its electronic, elastic, optical and thermal properties that make them suitable for possible applications in a variety of high

*Corresponding author: **M. A. R. Sarker, Email:**, razzaque_ru2000@yahoo.com
Department of Physics, University of Rajshahi, Bangladesh.

efficiency device applications. Aim of this study is to verify experimental observations using first-principle calculations [14].

2. COMPUTATIONAL METHODS

The simulation calculations presented in this work were carried out by employing Cambridge Serial Total Energy Package (CASTEP) code [15] which utilizes the plane-wave pseudopotential based on the framework of density functional theory (DFT) method. The electronic exchange-correlation energy is treated under the generalized gradient approximation (GGA) in the scheme of Perdew-Brike-Ernzerhof [16]. The interactions between the ions and electron are represented by ultrasoft Vanderbilt-type pseudopotentials for Co, Fe and O atoms [17]. The elastic constants are calculated by the 'stress-strain' techniques. The calculations use plane-wave cut-off energy 500 eV for all cases. For sampling of the Brillouin zone a Monkhorst-Pack grid [18] of 3×3×3 *k*-points were employed for all calculations. All the structures were relaxed by Broyden-Fletcher-Goldfarb-Shenno (BFGS) methods [19]-[20]. For the geometry optimization, the convergence tolerances were set as follows: 1×10^{-5} eV/atom for the total energy, 0.03 eV/Å for the maximum force on atoms, 0.05 GPa for the maximum stress, 0.001 Å for the maximum atomic displacement. In order to determine these thermodynamic properties for isotropic solid, Θ is expressed as in reference [21]

$$\Theta = \frac{\hbar}{K}\left[6\pi^2 V^{\frac{1}{2}} n\right]^{\frac{1}{3}} f(\sigma)\sqrt{\frac{B_s}{M}} \tag{1}$$

M being the molecular mass per unit cell and B_s the adiabatic bulk modulus. The static compressibility is given as described in reference [22].

$$B_s = B(V) = V\frac{d^2E(V)}{dV^2} \tag{2}$$

The thermal expansion coefficient, α and heat capacity C_v are given as

$$\alpha = \frac{\gamma C_V}{B_T V} \tag{3}$$

And

$$C_{V.vib} = 3nk\left[4D(\frac{\Theta}{T}) - \frac{3\Theta/T}{e^{\Theta/T}-1}\right] \tag{4}$$

Where γ is the Grüneisen parameter as described in [23] and is defined as:

$$\gamma = -\frac{d\ln\Theta(V)}{d\ln V} \tag{5}$$ (5)

The thermodynamic properties such as bulk modulus, Debye temperature, specific heats and volume thermal expansion coefficient are evaluated in the temperature range from 0 to 1000 K and in the pressure range from 0 to 50 GPa.

3. RESULT AND DISCUSSION

3.1. Electronic properties

We present the band structure and the densities of states (DOSs) of $CoFe_{2-x}M_xO_4$ [x=0.2; M =Zn, Zr & Cd] in Figs. 1 and 2, respectively. The valence and band overlap remarkably and many bands crossing the Fermi level. As a result, $CoFe_{2-x}M_xO_4$ [x=0.2; M =Zn, Zr & Cd] would demonstrate metallic conductivity which are in good agreement with experimental value [33].

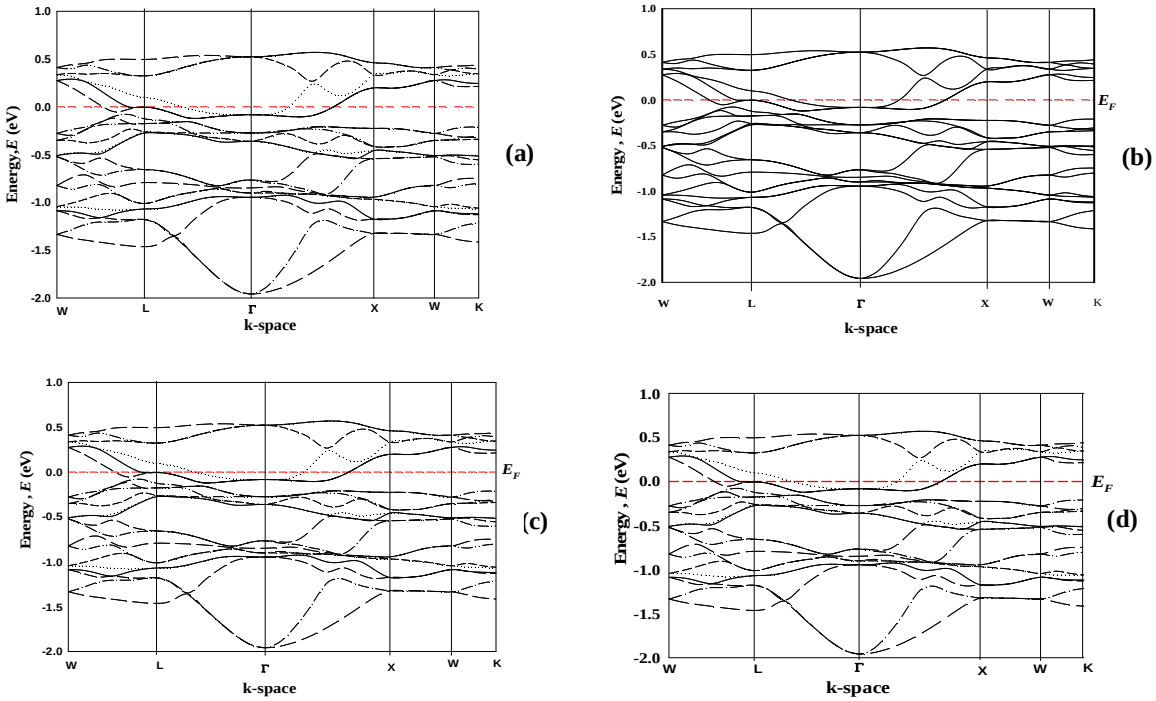

Figure 1 Electronic band structure for (a) $CoFe_2O_4$, (b) $CoFe_{1.8}Zn_{.2}O_4$, (c) $CoFe_{1.8}Zr_{.2}O_4$ and (d) $CoFe_{1.8}Cd_{.2}O_4$.

Fig. 2(a) shows that the lowest energy bands from -10 eV to -8.5 eV are mainly come from the Fe 3*d* states with little contribution from O 2*p* states. The energy bands between -8.5 and 0 eV are dominated by hybridizing Fe 3*d*, Co 3*d* and O 2*p* states. Fe 3*d* electrons are mainly contributing to the total DOS at the Fermi level and should be involved in the conduction properties. The value of total DOS at Fermi level is 19.28 states/eV. The highest contribution of partial DOS is for Fe 3*d* states and its DOS value is 11.82 states/eV. The DOS value at Fermi level reveals that $CoFe_2O_4$ is a conductor. This may now be compared with those for the total and partial electronic densities of states of $CoFe_{1.8}Zn_{.2}O_4$, $CoFe_{1.8}Zr_{.2}O_4$ and $CoFe_{1.8}Cd_{.2}O_4$ at zero pressure which are illustrated in Figs.2(b)-2(d). The values of total DOS at Fermi level for $CoFe_{1.8}Zn_{.2}O_4$, $CoFe_{1.8}Zr_{.2}O_4$ and $CoFe_{1.8}Cd_{.2}O_4$ are 19.83, 19.30 and 19.45 states/eV respectively. The highest contribution of partial DOS are Zn 3*d*, Zr 4*d* and Cd 4*d* states and their DOS values are 16.66, 16.27 and 16.23 states/eV. The DOS value at Fermi level reveals that doped $CoFe_2O_4$ are also conductor. Fig.2 shows that the total density of states at Fermi level of $CoFe_{1.8}Zn_{.2}O_4$ shifted effectively and that of $CoFe_{1.8}Zr_{.2}O_4$ and $CoFe_{1.8}Cd_{.2}O_4$ shifted slightly from non-doped $CoFe_2O_4$. Density of States for $CoFe_{2-x}M_xO_4$ [x=0.2; M =Zn, Zr & Cd] is given below in Table 1.

Table 1 Total and partial density of states for $CoFe_{2-x}M_xO_4$ [x=0.2; M =Zn, Zr & Cd] sample.

Compounds	Partial Density of States(States/eV)											Total DOS (States/eV)
	Co			Fe			O					
	3*p*	3*d*	4*s*	3*p*	3*d*	4*s*	2*s*	2*p*	Doping level (Dopant)			
$CoFe_2O_4$	0.42	4.91	0.05	0.07	11.82	0.12	0.08	2.29	undoped			19.28
$CoFe_{1.8}Zn_{.2}O_4$	5.02	0.07	0.46	0.08	11.62	0.15	0.14	2.43	Zn 3*p* 2.79	3*d* 16.66	4*s* 0.19	19.83
$CoFe_{1.8}Zr_{.2}O_4$	0.41	4.92	0.04	0.07	11.69	0.11	0.13	2.30	Zr 4*p* 2.73	4*d* 16.27	5*s* 0.25	19.30
$CoFe_{1.8}Cd_{.2}O_4$	0.39	4.90	0.03	0.09	11.34	0.14	0.11	2.31	Cd 4*p* 2.74	4*d* 16.23	5*s* 0.20	19.45

3.2. Elastic Properties

In order to study the mechanical properties of $CoFe_{2-x}M_xO_4$ [x=0.2; M =Zn, Zr & Cd], we have calculated the elastic constants C_{ij}, bulk modulus B, shear modulus G, Young's modulus Y, and Poisson's ratio σ. The calculated results are shown in Table 2. The sequence of hardness is reported to be $CoFe_{1.8}Zn_{.2}O_4$< $CoFe_{1.8}Zr_{.2}O_4$ < $CoFe_2O_4$ < $CoFe_{1.8}Cd_{.2}O_4$.This sequence shows that $CoFe_{1.8}Cd_{.2}O_4$ possesses a higher hardness due to its higher bulk modulus. The well-known Born stability criteria [25] involving elastic constants are: $C_{11} > 0$, C_{11}-$C_{12} > 0$, $C_{44} > 0$. It is seen that the born stability criteria are satisfied and hence they are mechanically stable under elastic strain perturbations. There are three elastic constants (C_{11}, $C_{12,}$ C_{44}) for all structures. The values of C_{11} for both $CoFe_{1.8}Zr_{.2}O_4$ and $CoFe_{1.8}Zr_{.2}O_4$ are higher than those of $CoFe_2O_4$, which show relatively larger resistances against the principal strain ε_{11}.The values of C_{11} for $CoFe_{1.8}Zn_{.2}O_4$ are smaller than those of $CoFe_2O_4$, which show relatively lower resistances. The C_{44}-value of $CoFe_{1.8}Zr_{.2}O_4$ is larger than that of $CoFe_2O_4$, which indicates higher resistances to basal and prismatic shear deformations compared to $CoFe_2O_4$.

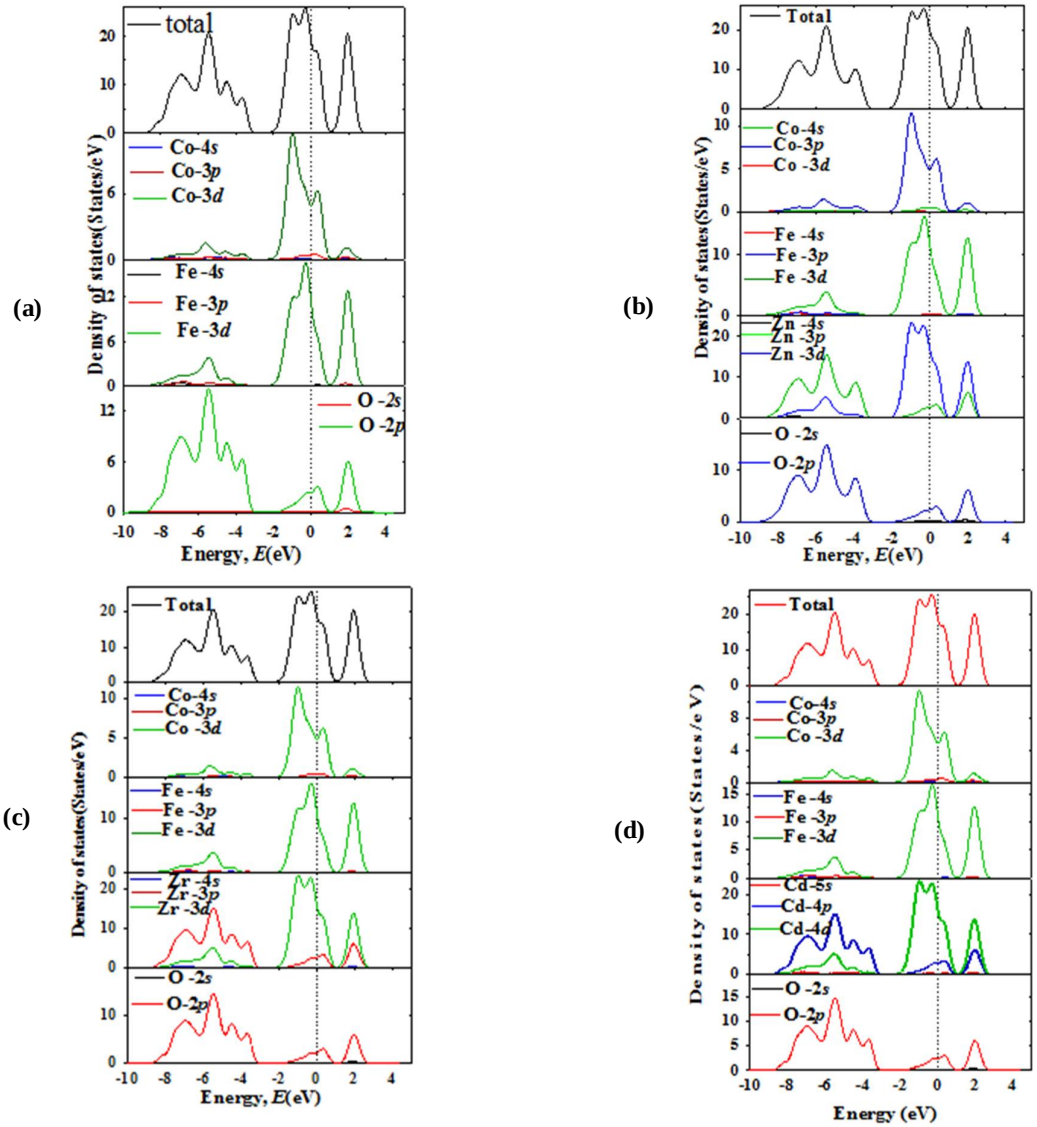

Figure 2 Total and partial density of states (DOS) of (a) $CoFe_2O_4$, (b) $CoFe_{1.8}Zn_{.2}O_4$, (c) $CoFe_{1.8}Zr_{.2}O_4$ and (d) $CoFe_{1.8}Cd_{.2}O_4$.

It is well known that crystals are usually prepared and investigated as polycrystalline materials in the form of aggregated mixtures of micro-crystallites with a random orientation. It is useful to estimate the corresponding parameters for the polycrystalline materials. The theoretical polycrystalline elastic moduli

may be calculated from the set of three elastic constants. According to Hill [26], the Voigt and Reuss equations represent upper and lower limits of the true polycrystalline constants.

The polycrystalline moduli are the arithmetic mean values of the moduli in the Voigt (B_V, G_V) and Reuss (B_R, G_R) approximation, and are thus given by Hill's bulk modulus, $B_H \equiv B = ½(B_R + B_V)$, where B_R and B_v are the Reuss's and Voigt's bulk modulus respectively. Hill's shear modulus, $G_H \equiv G = ½(G_R + G_V)$, where G_R and G_V are the Reuss's and Voigt's shear modulus, respectively.

Again the expression for Reuss and Voigt moduli can be found in Ref. [27]. The polycrystalline Young's modulus *Y*, and Poisson's ratioσ, are then found from these values using the relationships: $Y = 9BG/(3B + G)$, $\sigma = (3B - Y)/6B$ [28].

Table 2 The elastic constants C_{ij}, the bulk modulus *B*, Shear modulus *G*, Young's modulus *Y* (all in GPa), poission's ratio σ, anisotropic factor *A* and ratio G/B at zero pressure.

Compounds	C_{11}	C_{12}	C_{44}	*B*	*G*	*Y*	σ	*A*	*G/B*
$CoFe_2O_4$	387	126	133	233	49	125	0.41	1.19	0.21
$CoFe_{1.8}Zn_{0.2}O_4$	385	128	119	206	51	133	0.39	1.13	0.25
$CoFe_{1.8}Zr_{0.2}O_4$	420	73	70	224	46	86	0.44	2.00	0.20
$CoFe_{1.8}Cd_{0.2}O_4$	396	190	180	251	35	57	0.46	2.72	0.14

We note that the Young's modulus *Y* of $CoFe_2O_4$ is larger than that of other doped materials. Therefore, $CoFe_2O_4$ compared to other shows a better performance of the resistance to shape change and against uniaxial tensions.

The bulk modulus *B* of $CoFe_{1.8}Cd_{.2}O_4$ is higher than that of $CoFe_2O_4$.

The anisotropy factor, $A = 2C_{44}/(C_{11} - C_{12})$ is often used [29] to represent the elastic anisotropy of crystals. When A = 1, it represents elastic isotropy, while values greater or smaller than this measures the degree of elastic anisotropy. Table 2 shows that $CoFe_{2-x}M_xO_4$ [*x*=0.2; M =Zn, Zr & Cd] show completely anisotropic behavior.

Pugh's ductility index (*G*/*B*) is also used as a malleability indicators of materials [30]. If $G/B > 0.5$ the material will have a brittle, where as for $G/B < 0.5$ the material will have a ductile behavior. According to this indicator (Table 2), $CoFe_{2-x}M_xO_4$ [*x*=0.2; M =Zn, Zr & Cd] are ductile in behavior.

Finally, the obtained values of the Poisson's ratio, σ are 0.41 for $CoFe_2O_4$, 0.39 for $CoFe_{1.8}Zn_{.2}O_4$, 0.44 for $CoFe_{1.8}Zr_{.2}O_4$ and 0.46 for $CoFe_{1.8}Cd_{.2}O_4$. The Poisson's ratio for brittle covalent materials is small, whereas for ductile metallic materials it is typically 0.33 [31].

Thus the materials will show the characteristics of being more in the latter category.

3.3.Thermodynamic Properties

We present the temperature variation of isothermal bulk modulus of $CoFe_{2-x}M_xO_4$ [*x*=0.2; *M* =Zn, Zr & Cd] at zero pressure in Fig. 3(a). Our calculations show that *B* value is larger for Cd doping and smaller for Zr and Zn doping respectively. Results indicate that *B* decreases with increase of *T* at zero pressure. The decreasing rate is high for Zr doping.

Fig. 3(b) shows the pressure variation of room temperature bulk modulus. It is found that *B* increases with pressure at room temperature and decreases with temperature at zero pressure, which is consistent with the trend of volume.

The temperature dependence of Debye temperature, Θ_D of $CoFe_{2-x}M_xO_4$ [*x*=0.2; *M* =Zn, Zr & Cd] at zero pressure is displayed in Fig. 4(a).

We note that Θ_D is larger for Zn doped and almost flat. Θ_D is smaller in case of Zr and Cd doping respectively and decreases non-linearly with temperature.

The pressure dependent Debye temperatures at *T* = 300 K of $CoFe_{2-x}M_xO_4$ [*x*=0.2; *M* =Zn, Zr & Cd] are presented in Fig. 4(b). This shows a non-linear increase in case of Zr and Cd doping. Θ_D increases slightly up to 22 GPa and then decreases in cases of Zn doping.

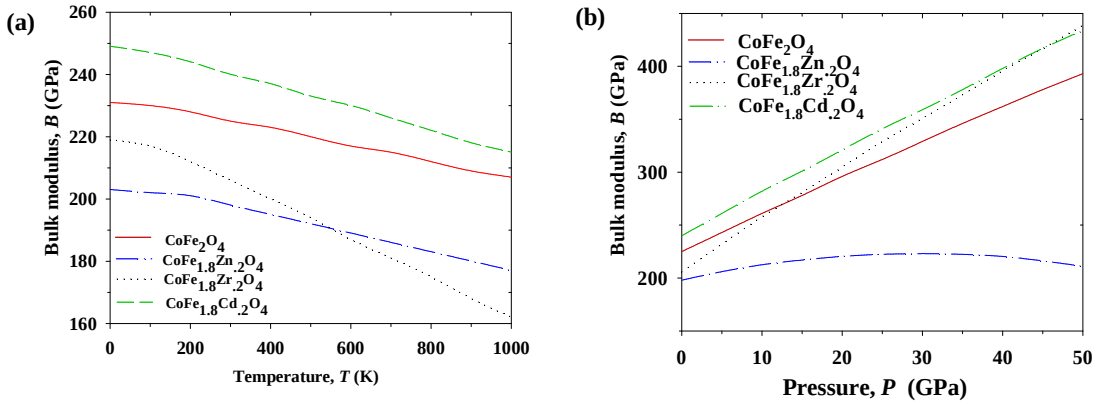

Figure 3 Temperature and pressure dependence bulk modulus of $CoFe_{2-x}M_xO_4$ [x=0.2; M =Zn, Zr & Cd].

However the variation of Θ_D with pressure and temperature reveals that the thermal vibration frequency of atoms in the nanolaminates changes with pressure and temperature. Also, the vibrational frequency is proportional to square root of the stiffness within the harmonic approximation; so Θ_D can be used to measure the stiffness of solids [32].

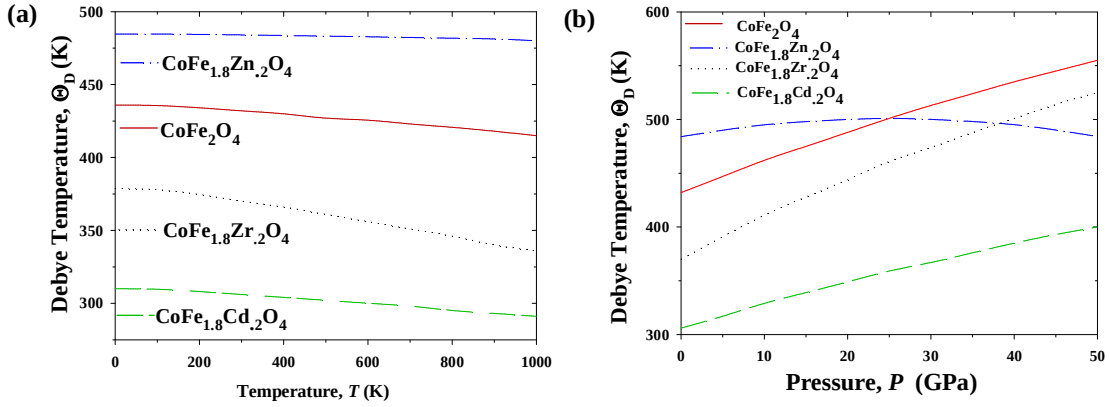

Figure 4 Temperature and pressure dependence Debye temperature of $CoFe_{2-x}M_xO_4$ [x=0.2; M =Zn, Zr & Cd].

In Figs. 5,6, the variation profiles of the heat capacity of $CoFe_{2-x}M_xO_4$ [x=0.2; M =Zn, Zr & Cd] with T and P are presented. As P = 0 GPa, at sufficiently low temperatures (T < 220 K), $CoFe_{2-x}M_xO_4$ [x=0.2; M =Zn, Zr & Cd] is proportional to (T=£D)^3.

It occurs because only the long wavelength vibration modes of the lattice are populated and these modes could be approximated by treating the lattice as a continuum. However, at high temperatures (T >220K), the an-harmonic effect on $CoFe_{2-x}M_xO_4$ [x=0.2; M =Zn, Zr & Cd] is suppressed and C_V is a constant which is in accordance with the law of Dulong and Petit. In this temperature range, the energy difference is less than the heat kinetic energy kT and it can be ignored in order to –t classical statistical theory. These curves show that C_V has classical behavior at high temperatures and quantum behavior at low temperatures. We also notice that pressure has also influence on heat capacity.

Specific heat decreases with pressure in case of Zr and Cd doping. Zn shows an anomalous behavior with pressure. However, the values of C_V become smaller and its changing trend becomes gentle and the range of agreement with Debye T^3 power-law becomes larger with an increase of pressure.

Again the values C_p are slightly larger than the values of C_v, due to the thermal expansion caused by anharmonicity effects and also which can be explained by the relation between C_p and C_v as follows:

$$C_P - C_V = \alpha_V^2(T)BVT \qquad (6)$$

Where, α_V = volume thermal expansion coefficient (VTEC) and B, V and T are the bulk modulus, volume and absolute temperature, respectively.

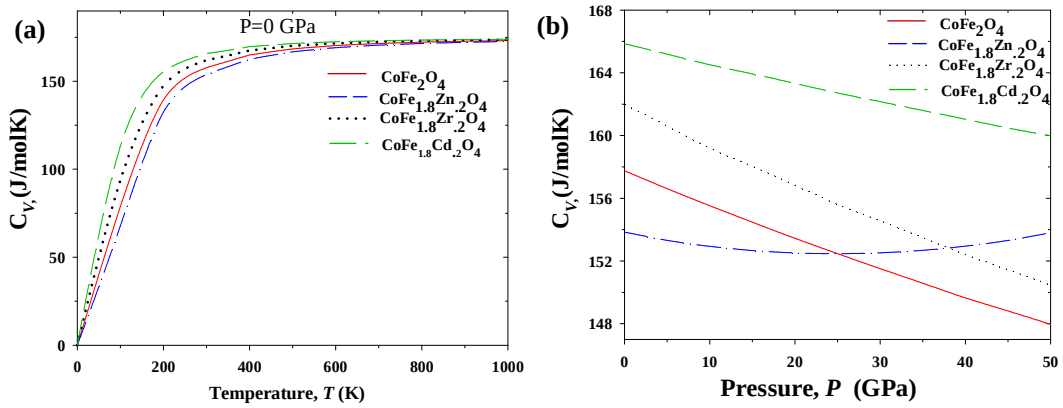

Figure 5 Temperature and pressure dependence specific heat at constant volume of $CoFe_{2-x}M_xO_4$ [x=0.2; M =Zn, Zr & Cd].

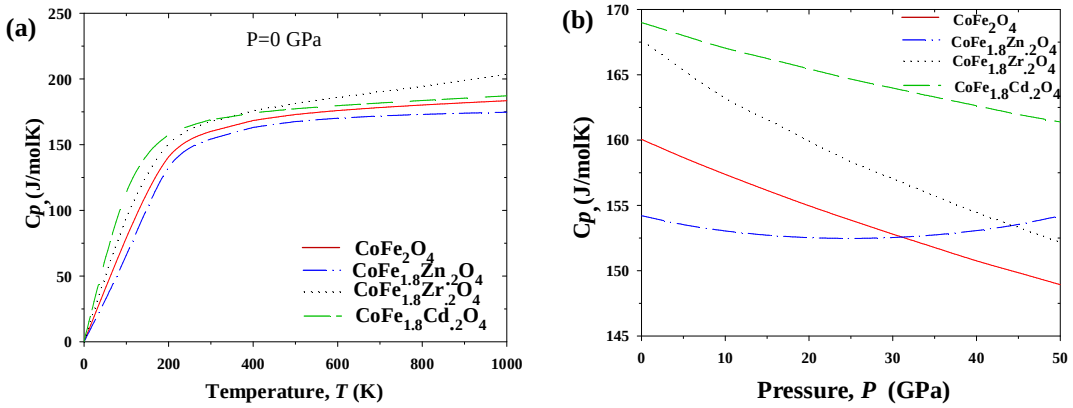

Figure 6 Temperature and pressure dependence specific heat at constant pressure of $CoFe_{2-x}M_xO_4$ [x=0.2; M =Zn, Zr & Cd].

3.4. Optical properties

Fig. 7(a) shows the volume thermal expansion coefficient (VTEC), α_V as a function of temperature for $CoFe_{2-x}M_xO_4$ [x=0.2; M =Zn, Zr & Cd] respectively. The thermal expansion coefficient remains constant up to 100 K and then decreases rapidly with temperature. The VTEC, α_V as a function of pressure is presented in Fig. 7(b). However at a constant temperature, the expansion coefficient increases strongly with pressure. It is also well-known that the thermal expansion coefficient is inversely related to the bulk modulus of a material.

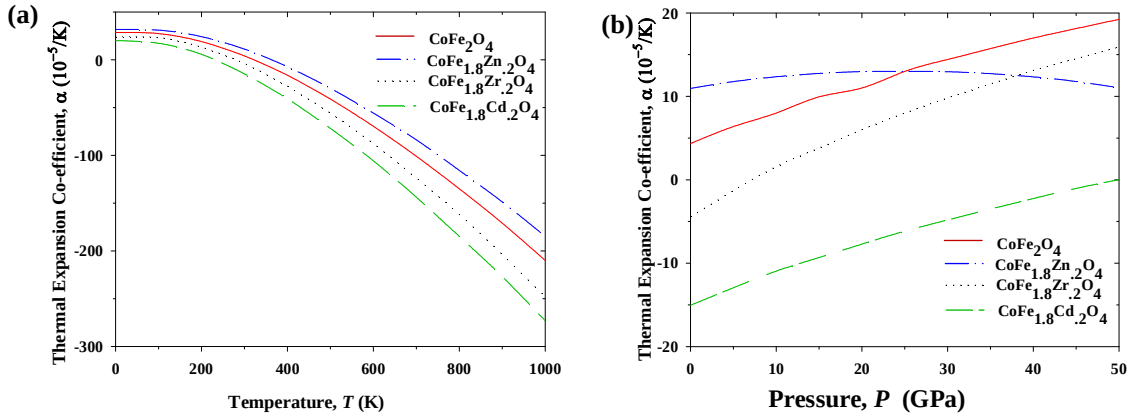

Figure 7 Temperature and pressure dependence thermal expansion coefficient of $CoFe_{2-x}M_xO_4$ [x=0.2; M =Zn, Zr & Cd].

To calculate the optical properties, we used a Gaussian smearing of 0.50 eV to smear out the Fermi level so that the k-points will be more effective on the Fermi surface. The real and the imaginary part of dielectric function of $CoFe_2O_4$ are shown in Fig. 8(a).

It is observed that the real part $\varepsilon_1(\omega)$ of the dielectric function vanishes at about 5eV. This corresponds to the energy at which the reflectivity exhibits a sharp drop at around 5 eV and the energy loss function shown in Fig. 8(d) also show the first peak. This peak in the energy loss function at about 5eV, which arises as ε_1 goes through zero and ε_2 is small at such energy. Thus this fulfils the condition for plasma resonance at 5 eV ($\hbar\omega_p$=5eV). The peak for <1eV for imaginary part ε_2 is due to transitions within the Fe 3*d* bands. The large negative values of ε_1 indicate that $CoFe_2O_4$ show Drude-like behavior.

The imaginary part (extinction coefficient, ***k***) and real part (refractive index, *n)* of complex refractive index are displayed in Fig. 8(b). The calculated value of static refractive index, n is zero at about 10 eV whereas for imaginary part of refractive index, k is zero at about 13 eV. The absorption spectra of $CoFe_2O_4$ are shown in Fig. 8(c). It has an absorption band in the low energy range due to its metallic nature. Its absorption spectra rise sharply and have two peaks at ~ 1.5 and ~ 3 eV. It then decreases rapidly up to energy ~ 4.5 eV. There is also a smaller peak at energy ~ 20 eV. The first two peaks are associated with the transition from the Co *d*/O *p* to the Fe *d* states. The loss function *L* (ω), for phases under study is displayed in Fig. 8(d), describes the energy loss of a fast electron traversing in the material [33]. Its peak is defined as the bulk plasma frequency ω_P, that occurs when ε_1 reaches the zero point [34]-[35]. In the energy-loss spectrum, we see that the plasma frequency ω_P of the $CoFe_2O_4$ is equal to 10 eV. Thus when the frequency of incident light is higher than ~ 10eV, the material becomes transparent. The reflectivity spectra as a function of photon energy are shown in Fig. 8(e). The reflectivity decreases with increase in photon energy up to 5eV and then increases. The reflectivity reaches maximum at 10 eV and then sharply decrease to zero. This result shows that this material may be used as promising coating material between 5 to 10eV. As the materials have no band gap as evident from band structure, the photoconductivity starts with zero photon energy as shown in Fig. 8(f). It has two peaks at 1 and 6eV. The photoconductivity and hence electrical conductivity of this materials increases as a result of absorbing photons [36].

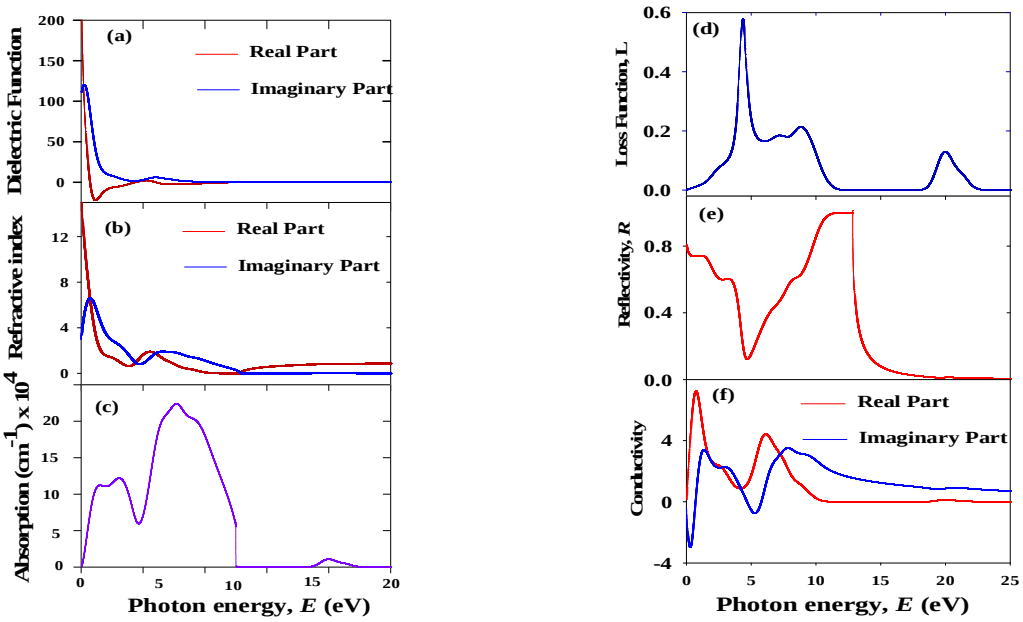

Figure 8 (a). Dielectric function (b) refractive index (c) absorption (d) loss function (e) reflectivity and (f) conductivity of $CoFe_2O_4$ samples as a function of photon energy.

4. CONCLUSION

First-principles calculations based on DFT have been used to study the electronic, elastic, thermodynamic and optical properties of $CoFe_{2-x}M_xO_4$ [x=0.2; M =Zn, Zr & Cd]. The elastic constants, bulk modulus, shear modulus ,Young's modulus bulk modulus, Debye temperature, specific heats, and volume thermal expansion coefficient (VTEC) are all obtained through the quasi-harmonic Debye model and are compared to those of other doped compounds. The electronic band structure in all cases shows metallic

conductivity. Moreover, the TDOS of Zn doped cobalt ferrite shifted effectively and show better metallic conductivity. The independent elastic constants are used to predict the mechanical stability which showed that all the compounds under consideration are stable. Cd doped cobalt ferrite possesses a higher hardness and ductility. Debye temperature increases with Zn doping. Finally, we see that C_v values are slightly smaller than the values of C_p, due to the thermal expansion caused by anharmonicity effects. The thermal expansion coefficient for all compounds increases strongly with pressure. Major changes occur in case of Zn doping. Cobalt ferrite has an absorption band in the low energy range due to its metallic nature. The reflectivity is seen to be high in visible-ultraviolet regions that can be used as a good coating material to avoid solar heating. The study should provide incentives for further experimental investigation which would pave the way for practical application for doped and non-doped $CoFe_2O_4$.

5. ACKNOWLEDGEMENTS

This work was partially supported by the Rajshahi University Research Grant (No. A774). Authors would like to thanks Rajshahi University, Rajshahi, Bangladesh authority for providing funds under the University Research Grant. Authors also would like to thanks Ministry of Science and Technology, Govt. of Bangladesh for providing scholarship to carry out this work.

6. REFERENCES

[1] K. Maaz, S.Karim, A.Mumtaz, S.K.Hasanain, J.Liu, J.L.Duan. 2009. J Magn. Magn. Mater. 321.
[2] Y. Ichiyanagi, M. Kubota, S. Moritake, Y. Kanazawa, T. Yamada and T. Uehashi. 2007. J. Magn. Magn. Mater. 310**:** 2378.
[3] Chen Y, Snyder J E, Schwichtenberg C R, Dennis K W, McCallum R W and Jiles D C. 1999 IEEE Trans. Magn. 35: 3652.
[4] Lisfi A and Williams C M. 2003. J. Appl. Phys. 93**:** 8143.
[5] Jeng H T and Guo G Y. 2002. J. Magn. Magn. Mater. 239**:** 88.
[6] Chinnasamy C N, Jeyadevan B, Shinoda K, Tohji K, Djayaprawira D J, Takahashi M, Justin Joseyphus R and Narayanasamy.2003. Appl. Phys. Lett. 83: 2862**.**
[7] Myrtil L. Kahn, Z. John Zhang. 2001. Applied Physics Letters. 78: 23.
[8] Jeng H T and Guo G Y. 2002. J. Magn. Magn. Mater. 239:88.
[9] P´enicaud M, Siberchicot B, Sommers C B and K ¨ubler J. 1992 J. Magn. Magn. Mater. 103: 212.
[10] Antonov V N, Harmon B N and Yaresko A N. 2003. Phys. Rev. B. 67**:** 024417.
[11] Walsh A, Wei S-H Yan Y, Al-Jassim M M and Turner J A. 2007. Phys. Rev. B. 76: 165119**.**
[12] Szotek Z, Temmerman W M, K ¨odderitzsch D, Svane A, Petit L and Winter H, Phys. Rev. B. 2006. 74: 174431.
[13] Md. Ashiqur Rahman, Md. Abdul Gafur, Md. Abdur Razzaque Sarker. 2015. IJIRAE. **2:** 99-107**.**
[14] S. J. Clark, M. D. Segal, M. J. Probert, C. J. Pickard, P. J. Hasnip, M. C. Payne, Z. Kristallor. 2005. vol. 220; 567-571.
[15] J. P. Perdew, K. Bruke, M. Ernzerhof. 1996. Phys. Rev. Lett. 77: 3865-3868.
[16] D. Vanderbilt. 1990. Phys. Rev. B. 41: 7892 – 7895.
[17] M. A. Blanco, A. Martín Pendás, E. Francisco, J. M. Recio and R. Franco. 1996. J. Molec. Struct. Theochem. 368: 245-255.
[18] E. Francisco, J. M. Recio, M. A. Blanco and A. Martín Pendás. 1998. J. Phys. Chem. A. 102: 1595-1601.
[19] M. S. Islam, A. K. M. A. Islam. 2011. Phys. B 406: 275-279.
[20] J.S. De-Almeida, R. Ahuja. 2006. Phys. Rev. B 73: 165102.
[21] M. A. Blanco, E. Francisco and V. Luan˜a. 2004. Comput. Phys. Comm. 158: 57-72.
[22] V. L. Moruzzi, J. F. Janak and K. Schwarz.1988. Phys. Rev. B. 3; 790799.
[23] M.Sc. Thesis, Md. Ashiqur Rahman, Department of Physics, University of Rajshahi (2015].
[24] Q. K. Hu, Q. H. Wu, Y. M. Ma, L. J. Zhang, Z. Y. Liu, J. L. He, H. Sun, H. T. Wang, Y. J. Tian. 2006. Phys. Rev. B. 73**:** 214116.
[25] R. Hill. 1952. Proc. Phys. Soc. London A. 65: 349.
[26] S. J. Clark, M. D. Segall, M. J. Probert, C. J. Pickard, P. J.Hasnip, M. C. Payne. 2005. Z. Kristallogr. 220: 567.
[27] A. Bouhemadou, Braz. 2010. J. Phys. 40: 52.
[28] I. R. Shein, A. L. Ivanovskii, arXiv: 1004. 1020.
[29] S. F. Pugh. 1954. Phil. Mag. 45: 823**.**
[30] M. S. Islam, A. K. M. A. Islam. 2011. Phys. B. 406:275-279.

[31] T. Tohei, A. Kuwabara, F. Oba and I. Tanaka. 2006. Phys. Rev. B. 73: 064304.
[32] R. Saniz, L. H. Ye, T. Shishidou, A. J. Freeman. 2006. Phys. Rev. B. 74: 014209.
[33] E. Francisco, J. M. Recio, M. A. Blanco and A. Martín Pendás. 1998. J. Phys. Chem. A. 102: 1595-1601.
[34] J.S. De-Almeida, R. Ahuja. 2006. Phys. Rev. B 73: 165102.
[35] M. Xu, S. Y. Wang, G. Yin, J. Li, Y. X. Zheng, L. Y. Chen and Y. Jai. 2006. Appl. Phys. Lett. 89:151908.